# First-Principles Determination of Hybrid Bilayer Membrane Structure by Phase-Sensitive Neutron Reflectometry

C. F. Majkrzak,* N. F. Berk,* S. Krueger,* J. A. Dura,* M. Tarek,*† D. Tobias,‡ V. Silin,§ C. W. Meuse,§ J. Woodward,§ and A. L. Plant§

*Center for Neutron Research, National Institute of Standards and Technology, Gaithersburg, Maryland 20899; †Department of Chemistry, University of Pennsylvania, Philadelphia, Pennsylvania 19103; ‡Department of Chemistry, University of California-Irvine, Irvine, California; and §Biotechnology Division, National Institute of Standards and Technology, Gaithersburg, Maryland 20899 USA

ABSTRACT The application of a new, phase-sensitive neutron reflectometry method to reveal the compositional depth profiles of biomimetic membranes is reported. Determination of the complex reflection amplitude allows the related scattering length density (SLD) profile to be obtained by a first-principles inversion without the need for fitting or adjustable parameters. The SLD profile so obtained is unique for most membranes and can therefore be directly compared with the SLD profile corresponding to the chemical compositional profile of the film, as predicted, for example, by a molecular dynamics simulation. Knowledge of the real part of the reflection amplitude, in addition to enabling the inversion, makes it possible to assign a spatial resolution to the profile for a given range of wavevector transfer over which the reflectivity data are collected. Furthermore, the imaginary part of the reflection amplitude can be used as a sensitive diagnostic tool for recognizing the existence of certain in-plane inhomogeneities in the sample. Measurements demonstrating the practical realization of this phase-sensitive technique were performed on a hybrid bilayer membrane (self-assembled monolayer of thiahexa (ethylene oxide) alkane on gold and a phospholipid layer) in intimate contact with an aqueous reservoir. Analysis of the experimental results shows that accurate compositional depth profiles can now be obtained with a spatial resolution in the subnanometer range, primarily limited by the background originating from the reservoir and the roughness of the film's supporting substrate.

## INTRODUCTION

Structures that serve as models of cell membranes are of fundamental importance in understanding such key biological processes as molecular recognition and self-assembly. The ability of neutron reflectivity to reveal information about the microstructure of biomimetic membranes has been demonstrated in a number of pioneering experiments (e.g., Fragneto et al., 1995; Vaknin et al., 1991), as well as in more recent studies (Koenig et al., 1996; Meuse et al., 1998; Fragneto et al., 2000; Kuhl et al., 1998; Blasie and Timmins, 1999). Most approaches have relied on fitting reflectivity data to compositional models with adjustable parameters or have used analytical schemes based on restrictive approximations. Such methods generally admit to multiple solutions and are uninformative about the spatial resolution of the results or of the quality of the sample that underlies them. In this paper we describe a systematic approach to determining the structure of biomimetic films along the surface normal using phase-sensitive measurements of neutron reflection and their direct inversion, which lead to unique compositional profiles with well-characterized spatial resolution and provide a collateral indication of sample film quality.

*Received for publication 20 June 2000 and in final form 20 September 2000.*

Address reprint requests to Dr. Susan Krueger, National Institute of Standards and Technology, Center for Neutron Research, 108 Bureau Drive, Stop 8562, Gaithersburg, MD 20899-8562. Phone: 301-975-6734; Fax: 301-921-9847; E-mail: susan.krueger@nist.gov.



0006-3495/00/12/3330/11 $2.00

The purpose of neutron reflectometry is to reveal the microstructure of materials in thin film geometries. Microstructure refers to structural variations on a length scale greater than atomic but inclusive of molecular length scales, i.e., a nanometer, for biological membranes. The coherent elastic scattering behavior of neutrons by the microstructure of a film is well-determined by a continuous scattering length density (SLD) function $\rho(x, y, z)$, which is a number density-weighted microscopic average of known isotope-specific constants (the scattering lengths) that characterize the interaction of neutrons with the film's atomic constituents. The lateral average, $\rho(z) = \langle \rho(x, y, z) \rangle_{xy}$ (with the $z$-axis normal to the surface), known as the scattering length density depth profile, causes specular reflection, in which incident and reflected beams make equal angles with the surface and lie in a plane perpendicular to it. Lateral variations of the microstructure can also cause nonspecular, or diffuse, reflection. Surface and interfacial roughness, embedded lateral inhomogeneities, and in-plane structure are potential sources of measurable diffuse reflection. For the membranes examined here, the diffuse component was, in fact, determined to be negligible.

The SLD profile $\rho(z)$ of a membrane relates directly to its chemical composition and can be interpreted with the aid of models or by comparison with molecular dynamics (MD) simulations. Since this profile determines the specular reflection from a film—the direct problem, it must be deduced from the measured specular reflectivity—the inverse problem. Because $\rho(z)$ is one-dimensional, the direct problem reduces to a one-dimensional scattering problem along the film normal, with wavevector transfer $Q = (4\pi/\lambda)\sin\theta$,

where $\lambda$ is the wavelength of the incident neutron beam and $\theta$ is the angle of incidence (reflection) relative to the plane of the film. Comprehensive reviews describing conventional neutron reflectometry can be found in the literature (Russell, 1990; Penfold and Thomas, 1990; Majkrzak et al., 1994). The specular reflectivity is the intensity of the specular beam, divided by the intensity of the incident beam, and is given theoretically by $R(Q) = |r(Q)|^2$, where $r(Q) = |r(Q)|\exp[i\phi(Q)]$ is the complex reflection amplitude, having modulus $|r(Q)|$ and phase $\phi(Q)$. In the direct problem we have, $\rho(z) \rightarrow r(Q)$, where $A \rightarrow B$ means that function $A$ is associated with (or produces) a unique function $B$. For a wide class of physically meaningful profiles, which includes the ones determined in this study, the inverse problem also has a unique solution, $r(Q) \rightarrow \rho(z)$. The inverse problem has unique solutions for all real-valued $\rho(z)$ that do not support bound states in the sense of quantum mechanics. This includes all $\rho(z)$ that are nowhere negative. Since hydrogen has a weakly negative scattering length, it may be possible for some SLD profiles with thick enough hydrogenous portions to have a bound state, but these situations can be anticipated and eliminated if need be by substituting some deuterium (large positive scattering length) for hydrogen. The solubility of the inverse problem generally requires that $\rho(z)$ be real-valued, i.e., nonabsorptive, which is true for neutrons to a high degree of approximation, except in rare cases. The methods described here assume that $\rho(z)$ is real. They do not apply, therefore, to x-ray reflectivity, in which $\rho(z)$ generally has a nonnegligible imaginary part. Conventional reflectometry, however, measures only $|r(Q)|^2$, which is insufficient for unique inversion. A simple example is the difference between a freestanding membrane SLD profile, $\rho(z)$, and its mirror image, $\rho(L - z)$, where $L$ is the thickness of the film. Both produce the same $R(Q)$ but different $r(Q)$; only the phase of reflection distinguishes one from the other.

In order to exploit the power of the inverse reflection problem as a means of finding $\rho(z)$, it is first necessary to have a reliable and practical way of determining the normally elusive $r(Q)$ from reflectivity measurements. Once this is in hand, the solution of the inverse problem proceeds straightforwardly in a two-step process. First, one computes the Fourier transform of the known $r(Q)$; let us call this function $G(z)$. Then this result becomes the input to an integral equation known as the GLM equation (Chadan and Sabatier, 1989) or, alternatively, to an equivalent partial differential equation (Sacks, 1993), whose solution produces $\rho(z)$. Because of the analytic properties of $r(Q)$, it turns out that $G(z)$ is real and can be computed either as the sine Fourier transform of Im $r(Q)$ or as the cosine Fourier transform of Re $r(Q)$ (Sacks, 1993). This freedom is useful to phase-determination reflectometry, because the surround variation method used in this work (Majkrzak and Berk, 1998) actually measures Re $r(Q)$ directly and unambiguously.

We obtain Re $r(Q)$ from two reflectivity measurements, in which the SLD values of the media fronting and backing the film are different (Majkrzak and Berk, 1998). The fronting medium is the medium in which the neutrons are incident and reflected; the backing medium is the transmitting medium, regardless of how the film is mechanically supported. The films studied here are hybrid bilayer membranes (HBMs), defined explicitly in Appendix A, and attached to a sputtered gold layer on a thick single crystalline silicon or sapphire substrate. The HBM consists of a monolayer of alkanethiol, which is associated with the metal through a sulfur-gold interaction, and a layer of lipid. The lipid leaflet of the HBM is always in direct contact with a thick aqueous reservoir, and thus is always fully hydrated. In this arrangement, since a thick reservoir would attenuate the neutron beam excessively, the neutrons are incident through the highly transparent substrate, which becomes, therefore, the fronting in these experiments. The films under study include the HBMs and their supporting gold layers. It has been shown (Majkrzak and Berk, 1998) that the reflectivities for films having two different frontings or two different backings can be algebraically combined at each accessible $Q$ to give Re $r(Q)$ for the film alone, as if it were free, with vacuum fronting and backing. Mathematically, the process entails simply solving two simultaneous linear equations for two unknown functions, $\alpha(Q)$ and $\beta(Q)$, which give Re $r(Q)$ as the point wise formula Re $r = (\beta - \alpha)/(\beta + \alpha + 2)$. As already mentioned, the (numerically approximated) cosine Fourier transform of Re $r(Q)$ then can be used to determine $\rho(z)$ for the free film. (For accuracy, we note that the procedure just described does not directly determine the phase of $r(Q)$, but rather what might be called an optimal combination of modulus and phase, *viz.*, Re $r(Q)$, for extracting $\rho(z)$. Once $\rho(z)$ is known, however, $r(Q)$, both its modulus and phase, can be computed from the direct problem. Technically, Re $r(Q)$ and Im $r(Q)$ are mutually determined through a dispersion relation, which is nonlocal in $Q$.)

We have described how $r(Q)$ can be obtained from two reflectivity measurements by the surround variation approach. It has long been the accepted view that determination of $r(Q)$ generally requires multiple measurements in which some part of the SLD profile of the sample is varied by the use of previously characterized reference layers (Lesslauer and Blasie, 1971) or by other known changes (Sanyal et al., 1993). (Some $\rho(z)$ exist, however, for which $r(Q)$ is functionally implicit in $|r(Q)|^2$, i.e., for which $|r(Q)|^2 \rightarrow r(Q)$ via a dispersion relation. Mirror symmetric SLD profiles, which satisfy $\rho(z) = \rho(L - z)$, comprise one such class (Berk and Majkrzak, 1996), but this is an exceptional case (Sacks, 1997). Other, more or less isolated examples are less well classified (Clinton, 1993), and there is no reliable way of knowing before the fact that the $\rho(z)$ which produced the measured $|r(Q)|^2$ has this property; for any such $\rho(z)$, one can construct an infinite set of $\rho(z)$ which

produce exactly the same $|r(Q)|^2$ but which have different $r(Q)$ (Reiss et al., 1996).) The early approaches, however, always relied on the use of the Born approximation or its extensions. (In the Born approximation, or kinematic theory, the assumption is made that the wave function inside the scattering medium can be approximated by that in free space. While asymptotically valid at large $Q$, where the reflectivity is small enough to justify the assumption, it fails catastrophically near the origin, where the reflectivity approaches unity and the wave function is appreciably distorted. Distorted wave extensions of the Born approximation can act to moderate its divergent behavior at $Q = 0$.) Recently, however, the phase problem for specular reflection has been exactly solved using reference layer protocols (Majkrzak and Berk, 1995; de Haan et al., 1995; Aktosun and Sacks, 1998; Aktosun and Sacks, 2000a,b; Lipperheide et al., 1998), and the practicality of some of these has been experimentally demonstrated (Majkrzak et al., 1998, 2000; Majkrzak and Berk, 1999; Schreyer et al., 1999). The surround variation method described above belongs to this general class of phase determination solutions, and because the references it employs are characterized by a single number, the SLD value for the variable fronting or backing, it is the simplest such approach, in principle. It should be pointed out that SLD contrast variation of an aqueous backing has been applied to the study of lipid bilayers by specular reflectivity (Fragneto et al., 1999), but in these experiments the resulting multiple data sets were analyzed by curve fitting; while this approach constrains the class of best-fit profiles, it is not equivalent to the exact determination of the complex reflection amplitude, which is required for genuine inversion.

Naturally, the quality of the data affects the SLD profile deduced from it, whether by phase determination and inversion (phase inversion) techniques or by fitting methods, and any one of a number experimental factors can have significant impact. For example, on a length scale smaller than the lateral coherence length of the neutron plane wave front (typically of the order of 100 $\mu$m), the roughness of the supporting substrate limits the spatial resolution of the measurement relative to that for a perfectly flat film—to the extent the roughness propagates through the film—even for perfect instrumental resolution. Whereas, on a length scale larger than the coherence length, a bent substrate degrades $Q$-resolution, distorting the SLD profile obtained from the measurement. Furthermore, the $Q$-range over which the reflectivity is measured limits the spatial resolution of $\rho(z)$. This is a direct effect in inversion methods, which require the Fourier transform of $r(Q)$, and will be illustrated below with examples from our experiments. In fitting analyses, on the other hand, the relationships between $Q$-range and the limits of reliable spatial resolution are less well characterized. In any case, subnanometer spatial resolution generally demands reflectivity measurements over six or more orders of magnitude of signal. This imposes significant restrictions on the amount of background that can be tolerated from scattering by the surrounding media, especially for films as thin as lipid bilayers. To a large extent, however, these factors can be limited or monitored. Technical details, essential for conducting the experiments described herein, including such topics as film deposition, sample environment, and instrument configuration, are given in a set of Appendices. Effects of counting statistics in phase-inversion analysis have been examined in simulated experiments (deHaan et al., 1995). The inversion problem is well behaved in this regard. In the experiments described here, counting uncertainties were unobtrusive.

We describe below the first application of the surround variation method of phase determination and inversion to an HBM to obtain its SLD profile. This result is then compared to the corresponding profile predicted by an MD simulation (Tarek et al., 1999) of a film of similar compositional structure. The analysis also provides a quantitative measure of the spatial resolution of the recovered profile. Finally, the phase information further provides a means of assessing the lateral homogeneity of the HBM film.

## APPLICATION OF PHASE INVERSION

### Measurement of the reflectivity

In order to implement the phase inversion procedure described in the Introduction, two sets of reflectivity data were collected for the THEO-$C_{18}$/*d*DMPC HBM. Sample preparation is described in detail in Appendix A. To provide the necessary surround variation, two different fronting media were effected by making the supporting substrate silicon for one data set and sapphire ($Al_2O_3$) for the other, as depicted in the inset of Fig. 1. As also shown in the inset, the incident beam entered, and the reflected beam exited, through the perpendicular sides of the substrate blocks. Such side entry eliminates complicating reflections from the other parallel surface of the substrate (Majkrzak et al., 2000). It would seem natural to vary the SLD of the aqueous backing by using different mixtures of light and heavy water components, since this could be done in place without having to prepare two samples. However, in this particular case, the SLD of the water-containing *d*DMPC lipid head group would also change if this were done, which would violate the central requirement of any reference method; namely, that the film of interest remain invariant.

Each of the full reflectivity curves shown in Fig. 1 required a collection time of approximately 15 h, including that needed for the background, to a maximum $Q$, $Q_{max}$, of 0.3 $Å^{-1}$. (In a series of related experiments concerning the adsorption of melittin in the HBM, useful reflectivity data were obtained to $Q_{max} = 0.7$ $Å^{-1}$ (Krueger, S., C. W. Meuse, C. F. Majkrzak, J. A. Dura, N. F. Berk, M. Tarek, and A. L. Plant, manuscript submitted for publication).) The procedure followed to minimize background is described in

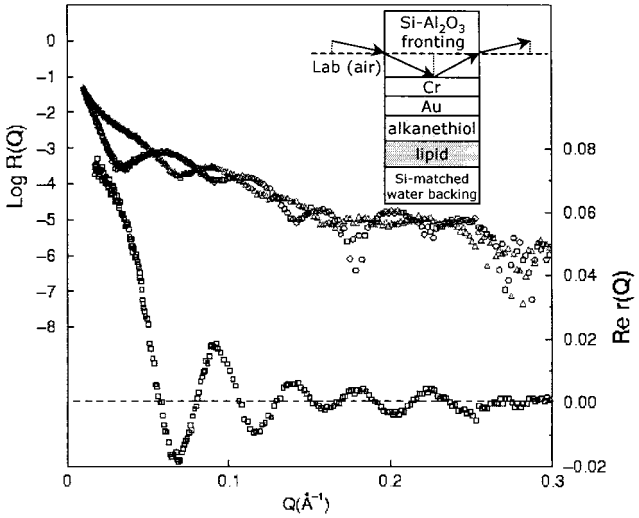


FIGURE 1 Reflectivity curves (referred to *left vertical axis*) for the thin film system depicted schematically in the inset, one for a Si fronting (*triangles*), the other for $Al_2O_3$ (*circles*). Note that the fronting medium is either Si or $Al_2O_3$. The real part of the complex reflection amplitude (*right vertical axis*, *squares*) obtained from these reflectivity curves by the method described in the text is also shown.

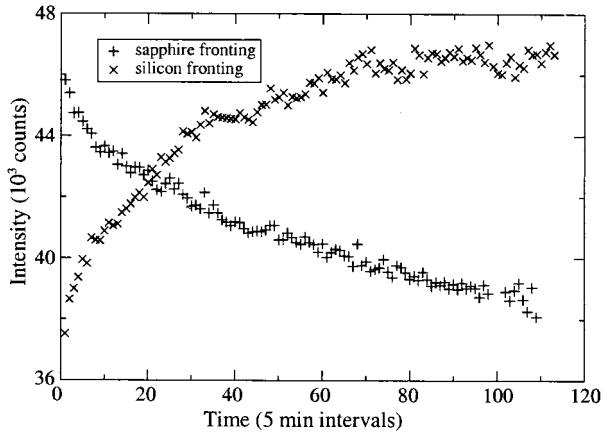


FIGURE 2 Time evolution of the self assembly of the lipid from vesicles as indicated by neutron specular reflectivity measured in situ at a fixed $Q$ of 0.0069 $Å^{-1}$. The data collection began approximately 15 min after the deposition process commenced.

Appendix B. Background scattering was collected at representative $Q$ values, defined by the glancing angle between the incident beam and the sample surface, with the detector or scattering angle offset from the specular condition (first on one, then on the other side of the peak). Several nonspecular scans were also performed to confirm that the diffuse scattering was negligible in comparison to the specular. The absolute reflectivity was obtained at each $Q$ by subtracting the background and then dividing by the incident beam intensity measured at zero scattering angle for the same slit settings. Instrumental details are given in Appendix C. The collection of the raw data and its subsequent reduction to reflectivity was done with a precision of 1% or better at the lower $Q$. Because of the limitations on counting time, the uncertainty in the measured reflectivity increases at higher $Q$, where the reflected intensity decreases dramatically.

Fig. 2 shows the reflected intensity at a fixed $Q$ (0.0069 $Å^{-1}$) as a function of time during the in situ self-assembly of the lipid layer from vesicles in solution (Appendix A). These particular data were collected in a subsequent repetition of the experiment. The time interval between successive data points is 5 min. The full specular reflectivity scans were not performed until equilibrium was reached, i.e., once the reflectivities at the fixed $Q$ shown in Fig. 2 stopped changing. The cell was rinsed with Si-SLD-matched water to remove vesicles from the subphase before the full scans were taken. In order to detect changes of the sample with time, once collection of complete reflectivity scans commenced, full reflectivity curves were repeated sequentially a number of times and compared. Identical scans then were combined to create a single composite reflectivity data set.

## Analytic determination of the real part of the complex reflection amplitude

The real part of the reflection amplitude, Re $r(Q)$, for the film, shown in Fig. 1, was obtained from the two reflectivity curves shown there using the surround variation procedure outlined above (Majkrzak and Berk, 1998). The method for extracting the reflection amplitude is local in wavevector transfer; at each $Q$, Re $r(Q)$ is correctly obtained from the two reflectivities at the same $Q$, independently of the reflectivities at other wavevector transfers. Thus, in particular, the accuracy of Re $r(Q)$ is unaffected by the finite range of $Q$ over which the reflectivity can be measured. On the other hand, in the inversion step, the accuracy of the resulting $\rho(z)$, which ultimately derives from a nonlocal transformation of Re $r(Q)$, does depend on $Q_{max}$, as will be discussed below.

Although reflectivity data are not available below some minimum value of $Q$ due to interference with the incident beam near zero scattering angle, an accurate interpolation of Re $r(Q)$ to $Q = 0$ can be made based on the film's net average SLD and thickness and the fact that Re $r(0) = -1$ for all $\rho(z)$ of interest.

## Inversion of the real part of the reflection amplitude to obtain the SLD profile

Fig. 3 shows the SLD profile, which results from the direct inversion of the Re $r(Q)$ plotted Fig. 1, together with the profile predicted by an MD simulation (Tarek et al., 1999). To show the effect of a finite $Q$ range on the inversion, a corresponding profile, also shown in Fig. 3, was generated

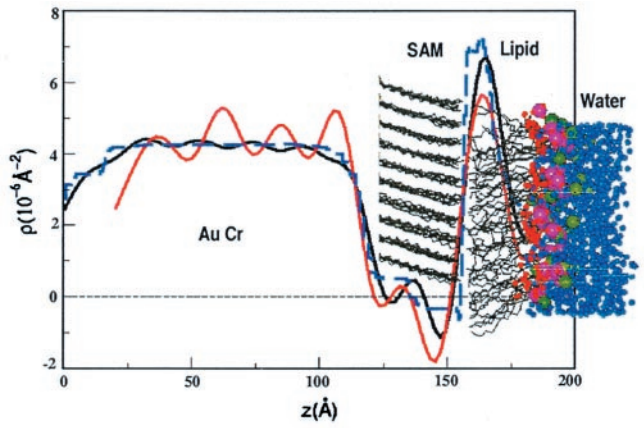


FIGURE 3 SLD profile (*red line*) resulting from a direct inversion of Re $r(Q)$ in Fig. 1, compared with that predicted by the molecular dynamics simulation (*dashed line*); note that the lipid considered in this simulation is DPPC. The SAM's head group in the experiment (ethylene oxide) was not included in the simulation, but rather modeled separately as part of the substrate. Also shown (*black line*) is the predicted SLD profile when the effects of data truncation are taken into account. Note that the protonated alkanethiol layer has a slightly negative SLD overall, whereas that of the deuterated phospholipid layer is strongly positive.

by inverting the Re $r(Q)$ computed for the $\rho(z)$ from the MD simulation, for the same $Q$-range over which the actual measurements were made.

The cosine Fourier transform, $G(z)$, of Re $r(Q)$, as required for inversion, was accomplished by ordinary numerical integration rather than by a fast Fourier transform. Our experiences with both approaches in simulated applications have indicated that the Nyquist spacing imposed by the fast Fourier transform degrades the spatial resolution inherent in $r(Q)$ up to a given $Q_{max}$, even when the sampling theorem is used to interpolate to a finer mesh. Also, to enhance the accuracy of $G(z)$ near the origin, where $G(0) = 0$, we actually performed a sine Fourier transformation of $-Q$ Re $r(Q)$ and then integrated this with respect to $z$ to obtain the requisite cosine transformation. The computed $G(z)$ was then inverted for $\rho(z)$ using the first of the two differential equation methods described in detail in Sacks (1993).

The result in Fig. 3 demonstrates remarkable agreement between simulation and measurement, to the extent permitted by the range of wavevector transfer over which reflectivity data were obtained. Both the thicknesses and SLDs of the metal layer components and the organic parts of the film shown in the figure are consistent with the values expected for these material constituents. Some of the oscillations of the SLD, especially evident on the gold layer plateau, are a result of the truncated reflectivity data sets, as shown below. The amplitudes of these oscillations, however, evidently are not completely accounted for by truncation.

Note that this SLD profile, obtained by first principles phase determination and inversion, is free of ambiguities normally associated with conventional curve fitting analyses, as is discussed in the following section.

## Spatial resolution and uncertainty in the inverted SLD profile

Besides eliminating the ambiguity and labor of curve fitting to produce a $\rho(z)$, phase inversion also can be implemented to assess the effect of data truncation, as mentioned above. In general, the uncertainty in the spatial location and magnitude of a particular feature in the SLD profile depends not only on the accuracy of the reflectivity, but also on the $Q$-range over which it is measured. The higher the value of $Q_{max}$, the better the spatial resolution of the inverted profile will be. However, because the real space of the inverted profile is related to the reciprocal space of the reflection amplitude by an integral transform, there is no pointwise correspondence between the two: what is localized in one space generally is distributed over the other. In particular, there is no simple relationship between the uncertainty of the reflectivity measured at a given $Q$ and that of the inverted SLD profile at a given depth (e.g., Lipperheide et al., 1996).

Nevertheless, the process of inverting Re $r(Q)$ induces a degree of uncertainty in $\rho(z)$ that is dependent on $Q_{max}$. Suppose that counting statistics are sufficiently good, $Q$-resolution is sufficiently tight, and systematic instrumental uncertainties are sufficiently small as to all have negligible effects on a phase-inverted profile. The only remaining ambiguity, then, is due to the spatial resolution of $\rho(z)$ imposed by a given $Q_{max}$. A series of comparative plots in Fig. 4 illustrates this effect for a model SLD profile similar to the HBM actually studied. Note that to resolve a spatial feature of length $D$, e.g., the splitting of the double peak structure at the far right of the profile in the figure, it is necessary to have $Q_{max} \approx 2\pi/D$, as expected from standard arguments. On the other hand, larger scale features can be less affected by the same truncation. For example, the overall thickness of the alkanethiol layer in Fig. 4, as defined by the distance between the half heights of the Au/alkane and alkane/lipid boundaries, is nearly independent of $Q_{max}$, at least for the ranges of $Q$ shown in the figure. A qualitative but convenient indicator of truncation effects is the ripple along the plateau of the Au layer. Both the magnitude and period of the oscillatory distortion increases with decreasing cutoff, and one can expect similar, though less obvious, distortions of other parts of the profile. On the other hand, as $Q_{max}$ increases, truncation effects die out and eventually disappear.

It is instructive in this context to consider in a bit more depth the implication of phase inversion and how it differs from conventional model dependent and model independent fitting procedures. Phase inversion effectively defines a one-parameter family of SLD profiles, $\rho(z|Q_{max})$, labeled by $Q_{max}$ and converging (almost everywhere) on the veridical, or true, profile—the one responsible for the measured reflectivity—as $Q_{max}$ approaches infinity. This family may be visualized as a curve in function space, in which points

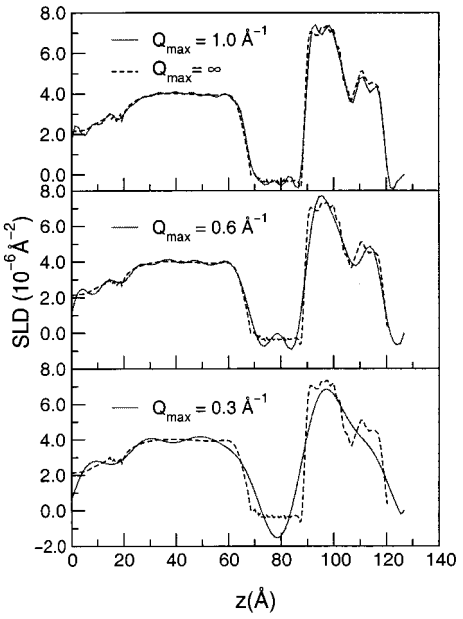


FIGURE 4 Scattering length density profiles obtained by inverting a calculated Re $r(Q)$ over different ranges of wavevector transfer $Q$ as compared to the original model SLD profile. The dashed line, corresponding to $Q_{max} = \infty$, is the same in all three graphs. The higher the maximum value of $Q$, the better the spatial resolution. This exercise provides a means of semi quantitatively assessing the spatial resolution of the resulting SLD associated with the finite range of a given reflectivity data set.

represent profiles. In experiments, $Q_{max}$ is made as large as feasible, but for a given $Q_{max}$, points along the curve are accessible at all smaller values of $Q_{max}$. In this sense, the phase inversion curve is revealed up to the experimental value of $Q_{max}$, which, along the curve, locates the profile closest to the veridical profile, situated at the terminus. Strictly speaking, the veridical profile, $\rho(z|\infty)$, is not directly measurable at finite $Q_{max}$, but it is known within the spatial resolution afforded by $Q_{max}$. Moreover, in the experiment, the rate of convergence along the phase inversion curve can be inferred by inverting the data at smaller values of the cutoff, as was described in the earlier examples.

One may attempt to locate the desired SLD profile in this function space by means other than phase inversion, such as by using model-dependent and model-independent fitting methods. Models define families of profiles of limited scope. A model function with a small number of parameters, even while being physically motivated, may not be descriptively rich enough to encompass the veridical profile. In this visualization of the function space, $\rho(z|\infty)$ would then lie outside the galaxy of best fits to the model in question. The best-fit galaxy of a good model may possibly hold a facsimile of the veridical profile, but the fitting process is unlikely to find it unless the starting point of the search is very close.

Model-independent fitting methods test data against general mathematical representations of SLD profiles drawn from suitably large function subspaces (Berk and Majkrzak, 1995), rather than testing against specific functions (models) suggested by theory or intuition. Model-independent fitting finds galaxies of profiles consistent with the data up to $Q_{max}$, which may include the veridical profile or a reasonable facsimile. Associated galaxies also exist, however, which contain symmetry-related profiles that generate the same or very nearly the same reflectivities. These galaxies cannot hold the true profile but are discoverable by model-independent fitting. Fig. 5 illustrates these behaviors with an example drawn from an actual experiment. As evident from the figure, it is possible to fit reflectivities with unphysical profiles.

With increasing $Q_{max}$, the accessibility of more data may contract the various fitting-scheme galaxies and draw some points metrically closer to $\rho(z|\infty)$, but only the phase inversion profile moves systematically toward the veridical profile along the phase inversion curve. It is possible that one or more profiles discovered by fitting at given $Q_{max}$ lie closer to $\rho(z|\infty)$ than does $\rho(z|Q_{max})$, but there is no way of knowing this without having other information.

## Imaginary part of the reflection amplitude as indicator of the in-plane homogeneity of the sample

As mentioned at the beginning, because of the planar geometry of a film, specular reflectometry reduces to the

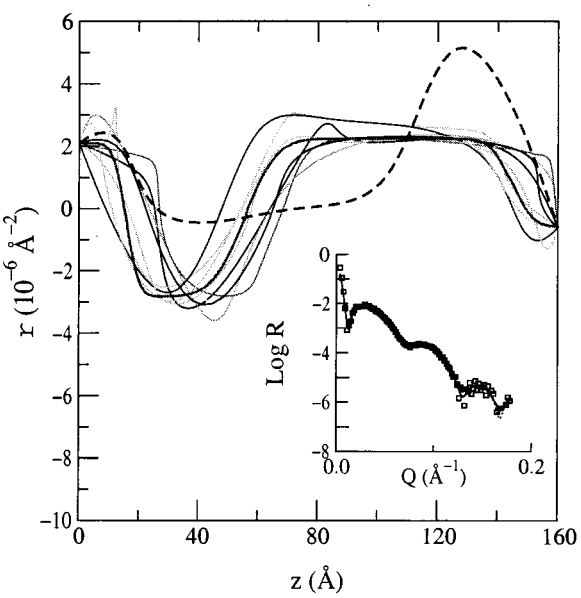


FIGURE 5 Family of scattering length density profiles obtained by model-independent fitting of the reflectivity data (*symbols*) in the inset. The profile represented by the dashed line is symmetry related but unphysical for this Ti/TiO film. The inset shows the corresponding reflectivities (*lines*), which are practically indistinguishable from one another. After Berk and Majkrzak (1995).

one-dimensional problem of finding the SLD depth profile along the surface normal. An essential premise of this special scattering arrangement is that the incident neutrons effectively average over lateral variations of the sample SLD over distances commensurate with the transverse coherence length of the incident beam, i.e., the distance over which the wavefront can be considered to be planar. Then coherent, specular reflection is a consequence of the interaction of the incident wave with the laterally averaged SLD, as described in the Introduction.

If in-plane regions of different SLD exist which have dimensions greater than the transverse coherence length (typically of the order of 100 $\mu$m in our work), then the measured reflectivity is incoherent, i.e., an area-weighted sum of separate reflectivities from each of these distinct regions, as illustrated in Fig. 6. There is no single physical SLD profile associated with such a composite reflectivity. Therefore, it is necessary to recognize the presence of lateral inhomogeneities in this dimensional regime.

Although it is true, as discussed above, that Re $r(Q)$ suffices to obtain $\rho(z)$ by inversion, it happens that Im $r(Q)$ is not completely redundant; indeed, it provides a means of establishing the existence of lateral inhomogeneities on a scale larger than the neutron coherence length (Majkrzak et al., 2000). It has been proven (Majkrzak et al., 2000) that for coherent specular reflection, Im $r(Q)$ always has a sequence of zeroes at $Q_n \approx n\pi/L$, where $L$ is the sample thickness.

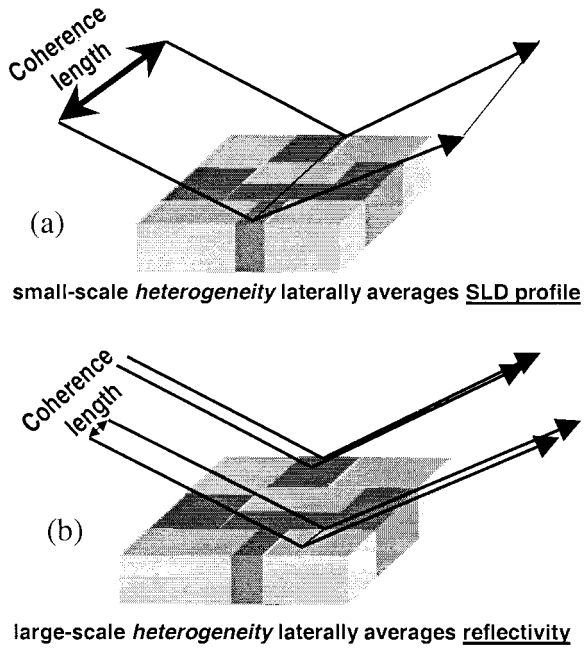


FIGURE 6 Schematic representation of the difference between coherent reflection from lateral inhomogeneities on a length scale smaller (*a*) or larger (*b*) than the neutron transverse coherence length. In case *a*, the measured reflectivity is produced by the corresponding laterally averaged SLD profile; in *b* it is the area-weighted superposition of reflectivities from each of the distinct lateral regions.

The occurrence of these zeros requires a physical $\rho(z)$, i.e., an effectively homogeneous film on the scale of the coherence length. An Im $r(Q)$ determined from data which is an incoherent average of reflectivities from separate homogeneous fractions generally will not exhibit a regular zero set. Thus, the absence of zeroes from an Im $r(Q)$ inferred from reflectivity data can be indicative of large-scale inhomogeneities. On the other hand, Re $r(Q)$ and the reflectivities from which it is derived fail to exhibit obvious signatures of this type of inhomogeneity (Majkrzak et al., 2000).

The diagnostic property of Im $r(Q)$ can be applied to the HBM described in this paper. In the course of the experiment, reflectivity measurements were repeated on different samples of the same system. On one occasion, the water in the aqueous reservoir was exchanged under a continuous flow for the duration of the reflectivity measurements. The intent was to minimize the possibility of gas bubble formation within the reservoir, which could cause lateral inhomogeneities of the kind considered above, i.e., some areas of lipid could be in contact with water, other parts with gas (air). Ironically, the fluid flow prevented visible bubble formation but also precipitated removal of patches of lipid. This was discovered by observing dramatic changes in the reflectivity after a relatively long time (24–36 h) under flow conditions. The reflectivity eventually became similar to that of the bare THEO-$C_{18}$ monolayer on Cr/Au, indicating the loss of the lipid layer. However, before enough lipid was removed to cause a large change in the reflectivity, two full data sets were collected out to $Q = 0.3$ Å$^{-1}$. The Re $r(Q)$ determined from these was qualitatively similar to that obtained previously, but upon inversion produced a profile in which the SLD of the lipid layer was substantially less than that consistent with complete coverage. However, inspection of the corresponding Im $r(Q)$, shown in Fig. 7, revealed an obvious reduction in the number of zeroes that should have been observed for this film. This is a definitive indication that this particular film was defective in a way rendering it unsuitable for further quantitative reflectivity analysis. Fig. 8, for comparison, shows Im $r(Q)$ for the original two reflectivity measurements, corresponding to the Re $r(Q)$ and $\rho(z)$ shown in Figs. 1 and 3, respectively, in which a static reservoir was used and no degradation of the lipid layer coverage occurred. Also plotted in Figs. 7 and 8 is the Im $r(Q)$ computed for the experimentally determined SLD profile in Fig. 3. The agreement between the two independent computations of Im $r(Q)$ demonstrates the internal consistency of phase inversion. In this example, it may be tempting to say that the film inhomogeneity ultimately was revealed by the SLD profile obtained, to the extent the result was not that expected for a good HBM film. It is important to emphasize, however, that although a putative $\rho(z)$ can always be defined for a bad film by a data analysis protocol, be it phase inversion or curve fitting, such a result is inherently unreliable.

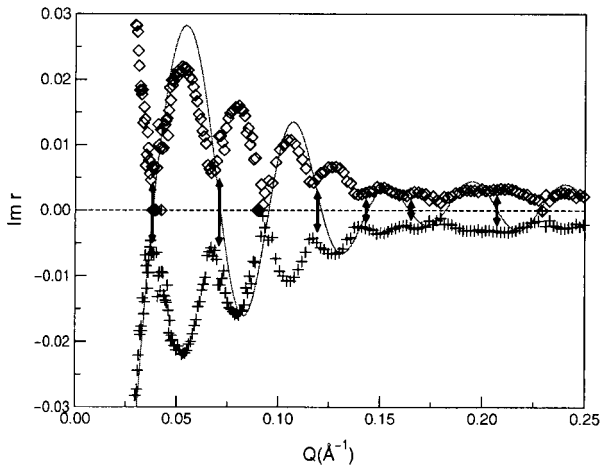


FIGURE 7 Putative Im $r(Q)$ (*symbols*) from reflectivity data in which partial lipid layer removal is suspected to have occurred under conditions of fluid flow through the cell. The Im $r(Q)$ calculated from the SLD of Fig. 3 is shown (*line*) for comparison and delineates the physical solution (Majkrzak et al., 2000). The depletion of the zero set, emphasized by the arrows, is argued in the text to indicate incomplete lipid layer coverage of the surface in this particular case.

## CONCLUSIONS

We have shown that phase-sensitive specular neutron reflectometry can be used to determine accurately and unambiguously the SLD depth profiles of biomimetic membranes with a resolution in the subnanometer range. The resulting profile can be compared directly with molecular dynamics simulations, from which a corresponding chemical compositional cross-section of the membrane can be deduced. The methodology, incorporating exact phase determination and first-principles inversion, also enables a systematic measure of spatial resolution. Finally, the properties of the imaginary part of the complex reflection amplitude, a byproduct of the procedure, allow certain in-plane inhomogeneities and other systematic defects to be identified.

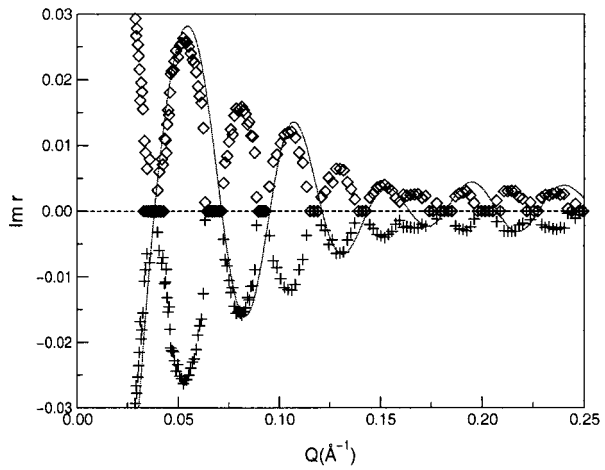


FIGURE 8 Im $r(Q)$ corresponding to the reflectivity data sets of Fig. 1 (*symbols*), compared to that associated with the SLD profile of Fig. 3 (*line*). See caption to Fig. 7. Note the relatively well defined zero set of the Im $r(Q)$ obtained from this measurement, which is consistent with complete lipid coverage.

In the study of the HBM described here, the nature of the samples required us to vary the fronting media in order to implement the surround variation method. This in turn necessitated the use of two different single crystal substrates. We currently are investigating the possibility of employing a single crystalline ferromagnetic support and a polarized beam, which would provide two fronting media (for two different spin polarizations) using a single physical specimen. We also note that although the current measurements were performed to $Q_{max} = 0.3$ Å$^{-1}$, better spatial resolution can be achieved by measuring out to $Q_{max} \approx 0.7$ Å$^{-1}$, which, as was mentioned above, has now been demonstrated for such films.

## APPENDIX A: SAMPLE PREPARATION

The hybrid bilayer membrane sample investigated here consists of a self-assembled monolayer (SAM) of HS-$(C_2H_4O)_6$-$(CH_2)_{17}$-$CH_3$ or [THEO-$C_{18}$] on a Cr/Au metallic bilayer, pre-deposited on single crystalline substrates, followed by a deuterated phospholipid layer *d*54-dimyristoyl phosphatidylcholine ($d_{54}$DMPC). The Au surface serves to chemically bond the SAM, to enhance the neutron reflectivity signal, and to act as an electrode in related electrochemical studies. Gold coatings about 100 Å thick were magnetron-sputtered simultaneously over a thin chromium adhesion layer (≈10 Å thick) on single crystalline sapphire ($Al_2O_3$) and silicon (Si) substrates in an argon gas atmosphere. Before the metal layer deposition, the substrates were washed in detergent solution, rinsed in water, and incubated in No-Chromix (Godax Labs, New York, NY) solution for 30 min. After extensive rinsing in high purity water (resistivity 18.2 MΩ), the substrates were washed with high purity acetone and dried in a nitrogen gas stream. An Edwards (Wilmington, MA) 306 vacuum system equipped with two (≈10 cm diameter) magnetron sputtering sources (one for chromium, the other for gold) was used for the metal film deposition on the clean silicon and sapphire substrates. The base vacuum level was better than $2 \times 10^{-5}$ Pa ($2 \times 10^{-7}$ mbar). The argon pressure, 0.1 Pa ($6 \times 10^{-3}$ mbar), was kept constant during the sputtering process using an MKS Instruments (Andover, MA) Baratron butterfly valve. Also, during sputtering the sample holder and samples were rotated over the gold and chromium targets (purity 99.99%) using a Superior Electric (Bristol, CT) SLO-SYN stepper motor system. A specially shaped mask was placed between the targets and the sample holder to ensure uniformity of film thickness over the whole sample surface. A DC power source was used at a power level of 750 W for gold and 440 W for the chromium depositions. The substrate rotation time required to produce a given film thickness was determined with the help of x-ray and neutron reflectivity measurements on test samples. Atomic force microscopy (AFM) measurements on freshly prepared samples indicated that the gold surface roughness was <2 Å rms. By measuring the light transmission through the gold on witness glass substrates, the homogeneity of the film across the substrate area was determined to be better than 99%.

For the data reported on in this paper, the substrates were flat discs approximately 7.62 cm in diameter and 0.3175 cm (⅛ in) and 0.47625 cm (3⁄16 in) thick for $Al_2O_3$ and Si single crystals, respectively. The crystallographic plane parallel to the surface is $(11\bar{2}0)$ for $Al_2O_3$ and (111) for Si. The sapphire was purchased from the Meller Optics Company (Providence, RI) and the Si from the Polishing Corporation of America (Santa Clara,

CA). Substrate as well as deposited film surface roughness is a contributing factor in limiting the spatial depth resolution attainable from specular reflectivity measurements. Specular x-ray reflectivity measurements indicated that the rms roughness for both of the crystal surfaces was in the range of 2 to 3 Å, approximately. Similar values were obtained from specular x-ray reflectivity and AFM measurements for the surfaces of the gold layers deposited on these substrates. The flatness of the substrate surface was determined, using x-rays and also neutrons, by measuring the rocking curve full width at half maximum (FWHM), wherein the glancing angle of incidence $\theta$ relative to the surface is varied at a fixed scattering angle of $2\theta$, about the specular reflection ridge in the vicinity of the critical angle. The FWHM was found to be of the order of 0.02° or less, limited by the instrumental angular resolution. Specular x-ray reflectivity measurements showed that the Au layer thicknesses on the $Al_2O_3$ and Si substrates differed by no more than about 1%.

The THEO-$C_{18}$ monolayers were prepared by immersing the gold-coated substrates in 0.25 mM thiol (Vanderah et al., 1998) solutions in 200 proof ethanol (Warner Graham Co., Cockeysville, MD) for a minimum of 12 h. In order to avoid the formation of multilayers, these surfaces either were soaked in 200 proof ethanol overnight or rinsed with tetrahydrofuran (Aldrich, Milwaukee, WI). The structure of monolayers formed this way has been published previously (Vanderah et al., 1998). The phospholipid used in these studies was $d_{54}$ (fully deuterated acyl chains) dimyristoyl phosphatidylcholine ($d_{54}$DMPC) from Avanti Polar Lipids (Alabaster, AL). Vesicle solutions were formed by injecting the lipid in isopropyl alcohol (2 $\mu$mol of lipid per 50 mL of isopropyl alcohol) into 1 mL of water (38% $D_2O$: Si SLD-matched water). These vesicles were then diluted to 10 mL Si SLD-matched water solution as described previously (Plant, 1993). The in situ formation of hybrid bilayers by this method has also been previously described (Hubbard et al., 1998; Petralli-Mallow et al., 1999). The in situ deposition on the neutron reflectometer was performed using the sample cell described in the next section. The formation of this $d_{54}$DMPC monolayer was monitored in real time by measuring the reflectivity at a fixed value of $Q$ as a function of time as already shown in Fig. 2.

## APPENDIX B: SAMPLE ENVIRONMENT AND CELL DESIGN

In order to extend the measurable $Q$ range as far as possible, so that the maximum spatial resolution in the SLD profile can be obtained, an acceptable signal to noise (S/N) ratio is required at reflectivities approaching the $10^{-7}$ or even $10^{-8}$ level. Of course, the greater the incident neutron beam intensity the better for this purpose. Nevertheless, this criterion alone is insufficient at large $Q$, where the signal is reduced to its lowest levels and background predominates. Background scattering from the media surrounding the sample becomes largest and especially problematical at higher $Q$ because the slits defining the incident beam are open widest at the corresponding angles, thereby illuminating more of the media surrounding the sample film with a more divergent beam (see the discussion on instrumental resolution in the next section). Here, to achieve a S/N ratio of at least O(1) requires that the incoherent scattering from the hydrogen present in the aqueous reservoir of the sample cell sandwich, pictured schematically in Fig. 1, as well as that from the gas surrounding the cell, be reduced to no more than a few counts per minute. At the NG-1 reflectometer in the NIST Center for Neutron Research guide hall where the measurements reported here were performed, the extrinsic (or room) background is, in comparison, negligible ($\leq$1 count per minute); so too is the contribution from the single crystalline parts of the cell defining the fronting and backing media. In practice, then, in order to achieve effective background suppression, the air surrounding the sample cell must be replaced with helium or argon gas (both of which have far smaller incoherent scattering cross sections) and the thickness of the aqueous reservoir must be minimized. It is worth pointing out that if an open secondary reservoir is used to gravity feed the cell reservoir, it is better to have it exposed to an argon rather than a He or air atmosphere, due to the lower solubility of the former gas in water. It is also essential to properly degas the aqueous solution to prevent the formation of gas bubbles in the cell reservoir which could affect the SLD of the backing medium, as discussed in the text in connection with lateral inhomogeneities.

The cell shown in Fig. 9 has a reservoir depth defined by the thickness of the gasket. The reservoir is filled with Si SLD-matched water and for a reservoir thickness of 25 $\mu$m, useful reflectivity data up to a maximum $Q$ of about 0.3 $Å^{-1}$ could be collected before the S/N ratio decreased appreciably below unity. Of course, if the experiment allows for an SLD closer to that of $D_2O$, then this can reduce significantly the amount of isotropic incoherent scattering for which hydrogen is the primary source. In related experiments (Krueger, S., C. W. Meuse, C. F. Majkrzak, J. A. Dura, N. F. Berk, M. Tarek, and A. L. Plant, manuscript submitted for publication), the use of an even thinner aqueous reservoir (about half the thickness) filled with pure $D_2O$ made it possible to collect useful reflectivity data beyond $Q = 0.7$ $Å^{-1}$. The cell has an inlet and outlet, each approximately 1.5 mm in diameter, drilled through the 0.9525 cm (⅜ in)-thick Si backing and through which aqueous solutions can be exchanged. In the experiment described in the text, heating of a brass block at the base of the cell, using a recirculating bath, maintained the temperature of the HBM and neighboring reservoir at approximately 28°C or a few degrees higher. Several disks, either all sapphire or all silicon, are stacked (after ensuring that the interfaces between adjacent discs are clean and dry) to form the incident medium as required for a particular reflectivity measurement.

## APPENDIX C: INSTRUMENTAL CONFIGURATION AND RESOLUTION

The NG-1 reflectometer at the NCNR operates at a neutron wavelength of 4.75 Å with a wavelength spread of approximately 1%. The scattering geometry is such that the reflecting surface of the sample is vertical and $Q$ therefore lies in a horizontal plane. The monochromator is situated in a gap of a rectangular guide tube approximately 15 cm high and 5 cm wide: the sides of the guide are coated with $^{58}$Ni and top and bottom with a Ni/Ti supermirror having a critical angle twice that of ordinary Ni. The monochromator is a vertically focusing type consisting of a mechanical device manufactured by Grenoble Modular Instruments (Grenoble, France) with seven individual, moveable magnesium fingers. On each finger a stack of three pieces of pyrolytic graphite, each piece with a crystal mosaic of roughly 20′ of arc, is mounted in a fanned-out arrangement such that the composite mosaic of the stack is about 1° in the horizontal plane. Each stack retains a 20′ mosaic in the vertical plane so that the monochromator has an effectively anisotropic mosaic better suited for vertical focusing of the incident beam on the sample, at a divergence of about 2.5°. By adjusting the width of a pair of vertical slits between monochromator and sample to be proportional to $Q$, both the footprint of the beam on the sample and the instrumental resolution $\Delta Q/Q$ remains approximately constant throughout a specular reflectivity scan. For a 4-cm footprint length in

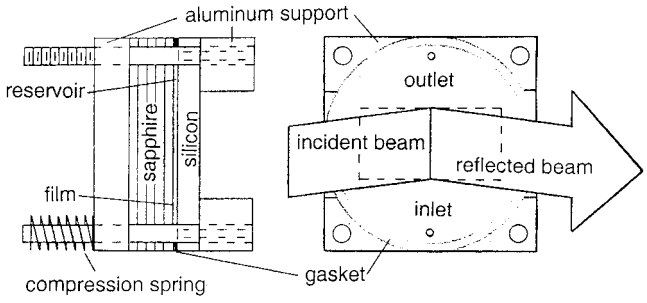


FIGURE 9 Schematic of the flow cell used in the reflectivity measurements involving phase determination. Details are given in the text.

the horizontal plane, $\Delta Q/Q$ is fixed at about 0.025. A polycrystalline Be filter, maintained at liquid nitrogen temperature, is placed between another pair of slits downstream of the sample and the detector in order to suppress higher order wavelengths reflected simultaneously by the monochromator. It is positioned here so that the broadening of the beam, produced by small angle scattering from the crystalline grains, does not affect the instrumental resolution. The slits following the sample are continually opened in conjunction with the pair upstream so that all of the divergent, specularly reflected beam is accepted at the detector. For the experiments on the film system described in the text, the instrumental $Q$ resolution was sufficiently high that it had negligible effect on the measured data, so that deconvolution was not necessary.

A careful alignment of the sample is performed in an iterative sequence in which incident angle, translation across the beam, and tilt from the vertical are successively optimized at a fixed scattering or detector angle at low $Q$ (below the critical angle if one exists for a particular combination of fronting and backing media). The flatness of a sample is judged to be acceptable if it does not broaden the reflected beam divergence significantly beyond that of the incident. It is sometimes necessary to rotate the substrate and/or fronting media discs about their common normal within the sample cell (typically in 45° increments) to obtain a proper seating, which does not produce deviations from flatness in excess of the minimum required. During the course of the specular reflectivity measurements, transverse or rocking curve scans are done periodically to ensure that proper alignment of the sample is being maintained.

In order to describe fully and accurately the materials preparation and measurement protocols of this research, it is necessary to mention certain commercial sources and products that were used. These references should not be construed as being endorsements by NIST nor should it be inferred that the products mentioned are necessarily the best available for the purpose.

## REFERENCES


Aktosun, T., and P. E. Sacks. 1998. Inverse problem on the line without phase information. *Inverse Problems.* 14:211–224.

Aktosun, T., and P. E. Sacks. 2000a. Inversion of reflectivity data for nondecaying potentials. *SIAM J. Appl. Math.* 60:1340–1356.

Aktosun, T., and P. E. Sacks. 2000b. Phase recovery with nondecaying potentials. *Inverse Problems.* 16:821–838.

Berk, N. F., and C. F. Majkrzak. 1995. Using parametric B splines to fit specular reflectivities. *Phys. Rev. B.* 51:11296–11309.

Berk, N. F., and C. F. Majkrzak. 1996. Inverting specular neutron reflectivity from symmetric, compactly-supported potentials. *J. Phys. Soc. Jpn.* 65 Suppl. A:107–112.

Blasie, J. K., and P. Timmins. 1999. Neutron scattering in structural biology and biomolecular materials. *Mater. Res. Soc. Bull.* 1999:40–47.

Chadan, K., and P. C. Sabatier. 1989. Inverse Problems in Quantum Scattering Theory, 2nd edition. Springer-Verlag, Berlin.

Clinton, W. L. 1993. Phase determination in x-ray and neutron reflectivity using logarithmic dispersion relations. *Phys. Rev. B.* 48:1–5.

de Haan, V. O., A. A. van Well, S. Adenwalla, and G. P. Felcher. 1995. On the retrieval of phase information in neutron reflectometry. *Phys. Rev. B.* 52:10831–10834.

de Haan, V. O., A. A. van Well, P. E. Sacks, S. Adenwalla, and G. P. Felcher. 1996. Toward the solution of the inverse problem in neutron reflectometry. *Physica B.* 221:524–532.

Fragneto, G., R. K. Thomas, A. R. Rennie, and J. Penfold. 1995. Neutron reflection study of bovine beta-casein adsorbed on OTS self-assembled monolayers. *Science.* 267:657–660.

Fragneto, G., F. Graner, T. Charitat, P. Dubos, and E. Bellet-Amalric. 2000. Interaction of the third helix of antennapedia homeodomain with a deposited phospholipid bilayer: a neutron reflectivity structural study. *Langmuir.* 16:4581–4588.

Hubbard, J. B., V. Silin, and A. L. Plant. 1998. Self-assembly driven by hydrophobic interactions at alkanethiol monolayers: mechanism of formation of hybrid bilayer membranes. *Biophys. Chem.* 75:163–176.

Koenig, B. W., S. Krueger, W. J. Orts, C. F. Majkrzak, N. F. Berk, J. V. Silverton, and K. Gawrisch. 1996. Neutron reflectivity and atomic force microscopy studies of a lipid bilayer in water adsorbed to the surface of a silicon single crystal. *Langmuir.* 12:1343–1350.

Kuhl, T. L., J. Majewski, J. Y. Wong, S. Steinberg, D. E. Leckband, J. N. Israelachvili, and G. S. Smith. 1998. A neutron reflectivity study of polymer-modified phospholipid monolayers at the solid-solution interface: polyethylene glycol-lipids on silane-modified substrates. *Biophys. J.* 75:2352–2362.

Lesslauer, W., and J. K. Blasie. 1971. X-ray holographic interferometry in the determination of planar multilayer structures. Theory and experimental observations. *Acta Crystallogr.* A27:456–461.

Lipperheide, R., G. Reiss, H. Leeb, and S. A. Sofianos. 1996. Aspects of the inverse scattering problem in neutron specular reflection. *Physica B.* 221:514–519.

Lipperheide, R., J. Kasper, and H. Leeb. 1998. Surface profiles from polarization measurements in neutron reflectometry. *Physica B.* 248: 366–371.

Majkrzak, C. F., J. F. Ankner, N. F. Berk, and D. Gibbs. 1994. Neutron and x-ray diffraction studies of magnetic multilayers. *In* Magnetic Multilayers. L. H. Bennett and R. E. Watson, editors. World Scientific, Singapore. 299–354.

Majkrzak, C. F., and N. F. Berk. 1995. Exact determination of the phase in neutron reflectometry. *Phys. Rev. B.* 52:10827–10830.

Majkrzak, C. F., N. F. Berk, J. Dura, S. K. Satija, A. Karim, J. Pedulla, and R. D. Deslattes. 1998. Direct inversion of specular reflectometry. *Physica B.* 241–243:1101–1103.

Majkrzak, C. F., and N. F. Berk. 1998. Exact determination of the phase in neutron reflectometry by variation of the surrounding media. *Phys. Rev. B* 58:15416–15418. (Erratum *Phys. Rev. B.* 60:16211.)

Majkrzak, C. F., and N. F. Berk. 1999. Inverting neutron reflectivity from layered film structures using polarized beams. *Physica B.* 267–268: 168–174.

Majkrzak, C. F., N. F. Berk, V. Silin, and C. W. Meuse. 2000. Experimental demonstration of phase determination in neutron reflectometry by variation of the surrounding media. *Physica B.* 283:248–252.

Meuse, C. W., S. Krueger, C. F. Majkrzak, J. A. Dura, J. Fu, J. T. Connor, and A. L. Plant. 1998. Hybrid bilayer membranes in air and water: infrared spectroscopy and neutron reflectivity studies. *Biophys. J.* 74: 1388–1398.

Penfold, J., and R. K. Thomas. 1990. The application of the specular reflection of neutrons to the study of surfaces and interfaces. *J. Phys. Condens. Matter.* 2:1369–1412.

Petralli-Mallow, T., K. A. Briggman, L. J. Richter, J. C. Stephenson, and A. L. Plant. 1999. Nonlinear optics as a detection scheme for biomimetic sensors: SFG spectroscopy of hybrid bilayer membrane formation. *Proc. SPIE.* 3858:25–31.

Plant, A. L. 1993. Self-Assembled phospholipid/alkanethiol biomimetic bilayers on gold. *Langmuir.* 9:2764–2767.

Reiss, G., and R. Lipperheide. 1996. Inversion and the phase problem in specular reflection. *Phys. Rev. B.* 53:8157–8160.

Russell, T. P. 1990. X-ray and neutron reflectivity for the investigation of polymers. *Mater. Sci. Rep.* 5:171–271.

Sacks, P. E. 1993. Reconstruction of step-like potentials. *Wave Motion.* 18:21–30.

Sacks, P. E. 1997. Recovery of singularities from amplitude information. *J. Math. Phys.* 38:3497–3507.

Schreyer, A., C. F. Majkrzak, N. F. Berk, H. Gruell, and C. Han. 1999. Using polarized neutrons to determine the phase of reflection from thin film structures. *J. Phys. Chem. Solids.* 60:1045–1051.

Sanyal, M. K., S. K. Sinha, A. Gibaud, K. G. Huang, B. L. Carvalho, M. Rafailovich, J. Sokolov, X. Zhao, and W. Zhao. 1993. Fourier reconstruction of density profiles of thin-films using anamalous x-ray reflectivity. *Europhys. Lett.* 21:691–696.

Tarek, M., K. Tu, M. L. Klein, and D. J. Tobias. 1999. Molecular dynamics simulations of supported phospholipid/alkanethiol bilayers on a gold (111) surface. *Biophys. J.* 77:964–972.

Vaknin, D., J. Als-Nielsen, M. Piepenstock, and M. Losche. 1991. Recognition processes at a functionalized lipid surface observed with molecular resolution. *Biophys. J.* 60:1545–1552.

Vanderah, D. J., C. W. Meuse, V. Silin, and A. L. Plant. 1998. Synthesis and characterization of self-assembled monolayers of alkylated 1-thiahexa (ethylene oxide) compounds on gold. *Langmuir*. 14: 6916–6923.